Assessment of the reactivity and hydration of Portland cement clinker phases from atomistic simulation: A critical review

J. Claverie, Q. Wang, Siham Kamali-Bernard, Fabrice Bernard

Assessment of the reactivity and hydration of Portland cement clinker phases from atomistic simulation: a critical review

Jérôme Claverie[a], Qianqian Wang[b], Siham Kamali-Bernard[c,*], Fabrice Bernard[c]

[a] *GeM, Research Institute of Civil Engineering and Mechanics, UMR CNRS 6183, Université de Nantes, France*
[b] *College of Materials Science and Engineering, Nanjing Tech University, Nanjing 210009, PR China*
[c] *Laboratory of Civil Engineering and Mechanical Engineering (LGCGM), INSA Rennes, Rennes, France*

Abstract

Over the last decade, atomistic simulations were increasingly employed to describe cementitious materials properties. As a complement to experimental measurements, they have improved our understanding of anhydrous and hydrated phases. This article reviews most of the principal investigations based on density functional theory, molecular dynamics, and related methods to assess the reactivity and hydration of Portland cement clinker phases at the nanoscale. Finally, the limitations of these methods are discussed, and alternative approaches and challenges are introduced.

Keywords: Portland cement. Clinker. Hydration. Reactivity. Density functional theory. Molecular dynamics. Electronic structure. Surface energy. Cleavage energy. Atomistic simulation. Tricalcium silicate. Dicalcium silicate.

1. Introduction

The hydration of Portland cement (PC) involves several processes from the dissolution/dissociation of molecular species to their precipitation and the formation of hydration products. PC is mainly composed by clinker which contains four main phases: alite, belite, aluminate, ferrite, whose pure forms are tricalcium silicate C_3S, dicalcium silicate C_2S, tricalcium aluminate C_3A and tetracalcium aluminoferrite C_4AF respectively. The hydration of PC produces principally portlandite (CH) and calcium silicate hydrates (C-S-H), and to a lower extent ettringite (AFt) and monosulfoaluminate (AFm). C_3S is the major constituent (50-80%) of PC clinker and the principal responsible for the strength development, in particular at early ages. After several minutes in contact with water, the initially fast dissolution rate of C_3S, characterized by a sharp exothermal signal on isothermal calorimetry measurements, drops down and remains slow during the induction period. The duration of this period depends on several parameters including the specific surface area [1]. Two main theories were proposed to explain the end of the induction period: a membrane theory

*Corresponding author
Email addresses: jerome.claverie@univ-nantes.fr (Jérôme Claverie), qqwang@njtech.edu.cn (Qianqian Wang), siham.kamali-bernard@insa-rennes.fr (Siham Kamali-Bernard), fabrice.bernard@insa-rennes.fr (Fabrice Bernard)

where metastable hydration products would form on the C_3S surface, thus hindering its dissolution; and a geochemical theory where the dissolution rate is controlled by undersaturation and reactive topography [2–4]. However, up to now, none of these theories was reproved and this question is still open [2]. While many studies indicate that dissolution is controlled by undersaturation [4–7], nanoglobular C-S-H structures were recently synthesized and might be representative of the metastable form which precipitates during the first minutes of hydration [2, 8, 9]. Therefore, quantifying the reactivity of PC clinker phases and understanding how they behave in contact with water represents a first step to explain the mechanisms behind the induction period and to make possible the design of additives and more sustainable binders.

With the growth of computational resources, atomistic simulation methods have increased their visibility in many research fields. Such methods have the significant advantage to simulate experiments that could not be carried out in laboratory because of their high cost or technological limitations. They can be divided into two levels of theory: quantum mechanics and classical mechanics. Quantum mechanical or first-principles methods involve the resolution of the Schrödinger equation by the way of approximations. Both Hartree-Fock and density functional theory (DFT) methods can be used to calculate the ground state energies of a many-body system with different approximation methods. In the Hartree-Fock scheme, the N-electron wave function is approximated to the Slater determinant of N one-electron wave functions composed of a spatial orbital and a spin function. In DFT, the variable function is the electron density, which only depends on three spatial coordinates. The many-body problem of 3N spatial plus N spin variables is thus reduced to 3 spatial variables. Hohenberg-Kohn theorems state that for any external potential, the ground state energy is a functional of the ground state density that can be determined by a variational method [10]. The self-consistent procedure to solve the variational problem was proposed by Kohn and Sham in 1965 [11] and is now implemented in a many programs. With the current computational power, DFT calculations are typically performed on systems of tens to a few thousands atoms. On the other hand, methods based on classical mechanics neglect the electronic motion and consider atoms as classical particles. The interactions between them are described by a force field (FF) consisting of a functional form and a set of parameters to calculate the potential energy of the system. FF parameters are generally optimized from experimental measurements and/or from quantum mechanics calculations. In Monte Carlo simulations, a physical property is calculated by sampling a statistical ensemble. The Monte Carlo method is probabilist: it does not consider thermal fluctuations explicitly but gives a statistical representation of the system at finite temperature. Conversely, molecular dynamics (MD) simulations, also based on statistical mechanics, can describe the evolution of a system over time. The motion of particles is calculated at each step by integration of Newton's equation of motion. The ergodicity hypothesis, important in MD, states that for a long enough trajectory, the time average of a physical property is equal to its ensemble average. Traditionally, physical properties are calculated during production runs, after the system has reached an equilibrium state, but it

is also possible to perform non-equilibrium simulations.

In order to accurately compute a given property, the FF itself and its parametrization are crucial. The *cemff* database provides information on the most reliable FF to simulate cementitious materials, including parametrization, benchmarks for geometric and elastic properties [12]. These FF are classified into two categories. The first category includes classical FF where covalent bonds are predefined and no reaction can occur during the simulation. Among these are ClayFF [13, 14], a general FF for clays, CSH-FF [15] a reparameterization of the original parameters of ClayFF, offering a more accurate description of C-S-H, CementFF [16–20] and INTERFACE FF (IFF) [21] which provides the most consistent parameters for tobermorite and various clinker phases [12]. The second category are reactive FF represented by ReaxFF [22, 23], for which Ca/O/H [24] and Si/O/H [25] sets of parameters were merged into a Si/Ca/O/H set [26], allowing the simulation of anhydrous and hydrated calcium silicate phases.

This review outlines the principal attempts to describe the reactivity and superficial hydration of clinker phases by mean of atomistic simulations. The reader should note that the MD simulation time cannot excess several nanoseconds, which is far from the timescale of the induction period and cannot even cover the initial dissolution period. However, atomistic simulations may give insights on reactivity based on electronic structure, or on the adsorption mechanisms of a single water molecule or a water film on clinker surfaces. Furthermore, the observations and results arising from these simulations could enable the elaboration of models at larger temporal and spatial scales. Only studies on the interaction of water with anhydrous cement phases are covered herein, and not the huge scientific effort made in the atomistic description of hydration products, especially C-S-H. It it is worth noting that the methods described herein were extensively employed to describe the aqueous interface of a wide range of common ionic minerals such as calcium carbonate [27–35], calcium sulfate [36, 37] and olivines [38, 39]. Moreover, most of the scientific publications on atomistic simulations of clinker phases regarding reactivity and hydration focus on C_3S and C_2S and only very few studies were reported on C_4AF and C_3A. This is why our review mainly focus on calcium silicate phases.

2. Reactivity of anhydrous clinker phases

2.1. Calcium silicate phases and their polymorphs

PC clinker has two calcium silicates phases: tricalcium silicate C_3S and dicalcium silicate C_2S. Their reactivity vary with the type and content of impurities. The higher reactivity of C_3S compared to C_2S is at the cost of a larger energy expense during manufacturing: the formation of β-C_2S from lime and quartz occurs at 963 K [39], and its reaction with lime at 1430 °C produces C_3S [40]. Investigations of phase transitions of pure C_3S up to 1100 °C revealed three triclinic, two monoclinic and one rhombohedral

polymorphs [41]:

$$T_1 \xleftrightarrow{620\,^\circ C} T_2 \xleftrightarrow{920\,^\circ C} T_3 \xleftrightarrow{980\,^\circ C} M_1 \xleftrightarrow{990\,^\circ C} M_2 \xleftrightarrow{1070\,^\circ C} R$$

In impure C_3S, the monoclinic M_3 polymorph stabilizes [42]:

$$M_1 \xleftrightarrow{990\,^\circ C} M_2 \xleftrightarrow{1060\,^\circ C} M_3 \xleftrightarrow{1070\,^\circ C} R$$

While C_2S (Ca_2SiO_4) only contains orthosilicates anions ${SiO_4}^{4-}$ and Ca^{2+}, C_3S (Ca_3SiO_5) also contains O^{2-} anions. It is worth to note that the current chemical abbreviations for cement phases are based on oxide compositions and do not depict their actual chemical constitution. Furthermore, according to the International Union of Pure and Applied Chemistry (IUPAC) nomenclature, Ca_3SiO_5 should be named tricalcium oxy silicate to account for its additional oxide anion compared to dicalcium silicate Ca_2SiO_4 [43]. Alite polymorphs mainly differ in the orientation of the silicate tetrahedrons, which may affect the coordination numbers of Ca and O atoms [41] and their hydration properties [44, 45]. Pure C_3S crystallizes in T_1 at room temperature [40], M_1 and M_3 are yet the most common forms of C_3S in industrial PC [46, 47]. Phase constitution experiments revealed that M_3-C_3S stabilizes with increasing MgO contents, while increasing the SO_3 content favour the stabilization of M_1-C_3S [46, 47]. A recent investigation has demonstrated that the M_1 content and compressive strength of alite paste can be optimized by controlling the SO_3/MgO ratio [45]. The M_3 polymorph was extensively used as a model for atomistic simulations. However, the M_1 polymorph crystal structure is still under evaluation since the results from high resolution synchrotron radiation [48], high temperature X-ray powder diffraction (XRD) [40], and transmission electron microscope (TEM) [45] for it are still needed to be synergistic.

C_2S exhibits four polymorphs on heating and five on cooling with the formation of the β polymorph, especially in the presence of impurities:

$$\gamma \xrightarrow{780\text{–}860\,^\circ C} \alpha'_L \xleftrightarrow{1160\,^\circ C} \alpha'_H \xleftrightarrow{1425\,^\circ C} \alpha$$

$$\gamma \xleftarrow{<500\,^\circ C} \beta \underset{630\text{–}680\,^\circ C}{\overset{690\,^\circ C}{\rightleftharpoons}} \alpha'_L \xleftrightarrow{1160\,^\circ C} \alpha'_H \xleftrightarrow{1425\,^\circ C} \alpha$$

The γ polymorph is structurally similar to olivine and is known to be less hydrophilic than β-C_2S. The interest in belite-rich sulfoaluminate cement is growing by reason of the lower energy consumption and the multiple sources of raw materials needed for its production, including industrial solid wastes [49–52]. Belite cements are also an alternative low heat cement with good durability properties. However, the activation of belite is crucial for the early-age strength development [53]. Such activation is generally obtained by annealing α-C_2S at low temperatures [54]. Furthermore, a recent investigation of β and α'_H-C_2S hydration products by scanning transmission X-ray microscopy revealed a higher hydraulic reactivity of the α'_H polymorph [55].

Apart from their lattice parameters and the symmetries of their crystal structures, the main difference between belite and alite is that the latter contains isolated oxide ions. First-principles calculations have shown that the higher reactivity of alite when compared to belite is due to the higher charge density localization of the valence band maximum around its isolated oxide ions [56, 57]. This opens a door to more investigation on the electronic structures and to the prediction of reactive sites of different alite and belite polymorphs.

2.2. Reactive sites prediction and impurity effect

Here are some definitions to facilitate the reader's comprehension:

- The density of states (DOS) is a probability density function that describes the number of states that can be occupied for at each energy level.
- The partial or projected density of states (PDOS) is the projection of the DOS on a specific orbital and describes the contribution of each orbital to the DOS.
- The local density of states (LDOS) is the spatial distribution of the DOS for a given energy level.
- The Fermi level is defined theoretically as the highest energy level occupied at 0 K.
- The valence band maximum (VBM) and conduction band minium (CBM) are defined by the band theory as the closest energy levels below and above the Fermi level respectively. The frontier molecular orbital theory defined the molecular orbitals corresponding to the VBM and CBM as HOMO and LUMO respectively.

Predictions of reactive sites are mostly carried out in bulk crystals by DFT calculations and assessment of the LDOS and PDOS of the VBM and CBM. The PDOS allows to identify the VBM and CBM, which corresponds to the atoms and orbitals the most likely to lose or withdraw electrons. The concept of Fukui function is a widely used local reactivity descriptor that describes the variation in electron density due to small changes in the number of electrons. Based on the frontier orbital theory, the Fukui function for the addition of an electron can be approximated to the electron density of the LUMO/CBM. Conversely, the Fukui function for the subtraction of an electron is approximated to the electron density of the HOMO/VBM [58, 59]. Therefore, the regions more susceptible to a nucleophilic attack are depicted by the LDOS of the CBM, while the regions more susceptible to an electrophilic are indicated by the LDOS of the VBM.

There is a significant difference between C_3S and C_2S regarding the distribution of the LDOS of the VBM that is localized around Oi atoms (isolated oxide anions) in C_3S and around Oc (oxygen atoms covalently bonded in orthosilicate anions $SiO_4{}^{4-}$) in C_2S (see Fig. 1). The depicted regions are therefore likely to lose

electron upon electrophilic attack and the fact that Oi atoms are loosely bound to the system suggests that they would react easier than Oc, thus explaining the higher reactivity of C_3S [56]. The oxygen atoms that would be the most likely to react upon electrophilic attack were also detected from the LDOS of the VBM in α', γ and β-C_2S [60]. In partial density of p-states of these oxygen sites, the gap between the peak of the highest occupied state and the Fermi level was smaller by 0.31 eV in β-C_2S than in γ-C_2S. Furthermore, a relationship was reported between lower stability and reactivity in belite polymorphs [61, 62]. In particular, the average Ca-Ca distance in the β and polymorph α' were ∼0.1–0.25 Å shorter than for γ-C_2S, making their structures less stable. Lower average distances between cations may indicate a larger repulsion and enhance the dissolution upon contact with water [61, 62]. Furthermore, non-bonding electrons dispersed on the p-orbitals of Oi and Oc in C_3S and C_2S were also determined and quantified by the integration of partial density of states at specified energy levels, stating that there are more non-bonding electrons in the M_1-C_3S (α'_L-C_2S) than in M_3-C_3S (β-C_2S), and that there is no non-bonding electron in the γ-C_2S [63].

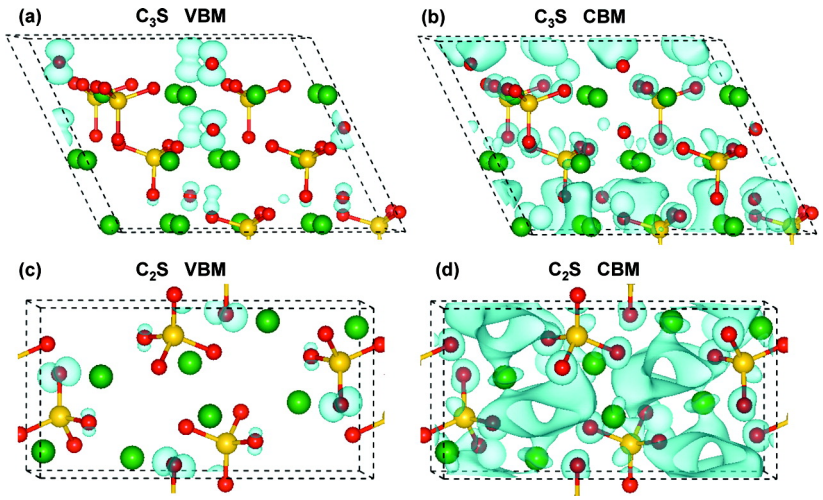

Figure 1: LDOS of the VBM and the CBM for (a), (b) M_3-C_3S, and (c), (d) β-C_2S. Green, yellow, and red spheres represent Ca, Si, and O atoms, respectively. Reprinted with permission from [56]. Copyright 2012 American Chemical Society.

As for C_3A, a DFT investigation reported that its reactivity originates from O-2p, Ca-3p, Ca-3s and Al-3p orbitals, and that the LDOS of the VBM and the CBM are localized in the vicinity of oxygen atoms and calcium atoms respectively [64, 65]. Such areas between calcium atoms are reactive to nucleophilic attacks and preferential adsorption sites for sulfate ions, which are highly nucleophilic [65, 66]. The occupation of these sites by sulfate ions could hinder the dissolution of C_3A and explain the retardation of PC hydration in the presence of gypsum [65–67]. DFT calculations on brownmillerite, the major constituent of C_4AF, reported that the LDOS of the VBM is localized at the vicinity of oxygen atoms, while the LDOS of the CBM is mainly localized on Fe atoms [68, 69]. These studies suggested that oxygen atoms in the Fe octahedral

plane would be the most likely to suffer electrophilic attack [68, 69].

It is well known that impurities affect the reactivity of clinker [40], Mg, Al or Fe being the most common in calcium silicate phases. Controlling the reactivity of clinker phases is of special interest for the cement industry. In particular, increasing the reactivity of belite could enable the design of new cement types, with lower carbon and energy footprints [56, 70]. In alite, Mg^{2+} substitution is predominant, and Al^{3+} and Fe^{3+} are secondary, whereas that trend is reversed for belite [40, 70]. Several studies provided a reactivity analysis of cement phases from classical FF and/or DFT calculations on bulk crystals by assessing the influence of minor and major impurities on the lattice energy, the LDOS of VBM and CBM, the total and partial density of states, the charge localization and the number of non-bonding electrons on oxide ions [56, 63, 70–72]. In some of these studies, substitutions of Ca^{2+} by Mg^{2+} did not affect considerably the LDOS of the VBM and CBM, whereas substitutions of $Ca^{2+} + Si^{4+}$ for $2\,Al^{3+}$ or $2\,Fe^{3+}$ had considerable effect on it [56, 70]. The stronger charge localization of Al-doped systems compared to Mg-doped system induced more reactive region for nucleophilic attack but decreased the spread of the LDOS of the VBM and CBM [56, 71]. These two contrary effects could explain conflicting experimental results [73–75]. For Fe-doped C_2S and C_3S, a metallic-like band structure was observed with a strong charge localization on the impurity, thus reducing drastically the number of reactive regions [56, 71]. All these studies agreed on the fact that Fe impurities in C_3S would depressed reactivity [56, 63, 70, 72]. In addition to the lattice energy, the enthalpy of formation of pure and impure phases provided information on the stability of doped phases. For belite and M_3-C_3S, computed lattice energies increased (in absolute value) with the incorporation of Mg^{2+}, suggesting more stable phases, but decreased with the incorporation of Al^{3+} and Fe^{3+} [70]. For T_1-C_3S, the lattice energy and enthalpy of formation decreased with incorporations of Mg, Al and Fe, indicating a lower stability of doped phases [72]. In all cases, the lattice energy and enthalpy of formation varied in a linear fashion with the impurity content [70, 72]. Furthermore, a systematic investigation on the defect formation of several dopants pointed out the influence of the ionic size mismatch between the dopant and the substituted ion on the destabilization of the β-C_2S structure [76].

Other metals coming from refuse-derived fuel and secondary raw materials can incorporate during the clinkering process. Based on DFT calculations, the stability and reactivity variation arising from Mn and Zn impurities in clinker phases were assessed using similar methods [77, 78]. While the incorporation of Zn reduced dramatically the number of reactive sites in C_3S and C_3A, it may promote the reactivity of C_4AF [78]. The defect formation energies indicated that the substitution of Mn or Zn for Fe in C_4AF was the most favorable [78, 79]. This is in agreement with experimental observations of reduced amounts of C_3A in Zn-doped clinkers, suggesting that substituted Fe may react with C_3A to form C_4AF [79, 80].

2.3. Surface energy and Wulff shape

By definition, the surface energy is the excess energy associated with a surface [81]. The energy needed to split a crystal along a specific plane is referred to as cleavage energy. It is therefore the average of the energies of the two surfaces of a crystal slab model. A practical way to simulate a surface model consists in creating a box with three-dimensional periodicity, composed by a slab in contact with a vacuum gap. The thickness must be sufficient so that the properties of the center of the slab converge to those of the bulk, and the vacuum region needs to be large enough such that the surfaces do not interact through the boundaries. The cleavage energy is commonly computed as the difference between the slab and the bulk energies, divided by the generated surface area:

$$E_{cleav} = \frac{E_{slab} - E_{bulk}}{2A} \tag{1}$$

where E_{slab} and E_{bulk} are respectively the energies of the slab system and the bulk system, with the same stoichiometry and number of atoms, and A is the surface area of one side of the slab. The bulk energy is typically computed on a unit cell or a supercell. Another way mostly used in MD simulations to compute the cleavage energy is to subtract the energies of a unified slab and a cleaved slab, using the following equation:

$$E_{cleav} = \frac{E_{cleaved} - E_{unified}}{2A} \tag{2}$$

When the surfaces on both sides of the slab are symmetrically equivalent, the surface energy is equal to the cleavage energy. However, most minerals do not fulfill this condition for all Miller indices. Among various existing methods to compute the surface energy, Manzano et al. [82] suggested to divide the slab in contact with a vacuum into two atomic groups. Both groups have one side exposed to the vacuum region and the other in contact with the other group. The surface energy of each side of the slab can be computed as follow:

$$E_{surf} = \frac{E_{slab} - E_{bulk}}{A} \tag{3}$$

A particular attention is needed on the atomistic model to employ for surface energy calculations, and especially regarding the distribution of ionic species on each surfaces [81, 83]. Tasker classified the surfaces of ionic crystals into three types [81]:

- type 1: surfaces consisting of coplanar cations and anions, resulting in a zero dipole moment
- type 2: surfaces consisting of a stacking of cationic and anionic layers, where the combination of layers hence leads to a zero dipole moment
- type 3: surfaces for which the stacking sequence of charged layers leads to a non-zero dipole moment. Such surfaces cannot be stable without a reconstruction involving the displacement of ions from one side to the other or by adsorption of additional charge

One should note that calculations on asymmetrical, non-reconstructed Tasker's type 3 surfaces are not in accordance with the classical electrostatic criteria [81, 84] and could lead to unrealistic charge distribution when performed by DFT or reactive force field.

Surface growth or formation are based on free energy minimization [85]. The undercoordination of superficial atoms results in rearrangements and changes in electronic structure. Dangling bonds on surfaces tend to localize the electronic charge and are susceptible to suffer chemical attack from adsorbates [82, 86]. In general, high surface energies are associated with unstable surfaces with low coordination number of superficial atoms. Such surfaces would create strong bonds with external species to minimize their energy [82]. However, the different bonding nature of superficial monoatomic ions in β-C_2S and M_3-C_3S compared to the bulk resulted in a reversed trend in a DFT investigation where coordination numbers of Ca^{2+} and O^{2-} ions were inversely proportional to the surface energy [87]. The lowest surface energies of pristine C_3S, C_2S and C_3A computed in each direction are reported Table 1. Since multiple cutting planes can be considered to build surface models in each direction, surface energies of M_1 and M_3-C_3S for different shift are also reported in Table 2. Despite a significant variability between data from different studies for specific planes, the overall range of surface energies are consistent. Unexpectedly, lower surface energies were obtained for β-C_2S than for γ-C_2S despite the former is known to be more reactive to water [39]. Furthermore, the effect of impurities on the surface energy of the T_1-$C_3S(100)$ plane was investigated and resulted in 0.9% and 2.5% decreases for Al and Mg substitutions respectively, while Fe doping induced a significant reduction of 7.9% [88]. Discrepancies between the data may arise from two different sources. The first one is the construction of the surface model with regard to the sizes of the slab and the vacuum, as well as the arrangements of superficial atoms – a particular attention is needed for reconstructed surfaces. The second source of discrepancy are the computational methods and parameters employed – i.e. empirical force field for MD, and exchange-correlation functional, basis functions and k-point sampling for DFT calculations. For the sake of reliability, it should be interesting to repeat calculations, verifying the convergence of surface energy for every plane and giving particular attention to the construction of Tasker's type 3 surface planes.

While cubic and orthorhombic forms of impure C_3A are commonly present in industrial PC, pure C_3A only exists as a cubic crystal made of Al_6O_{18} rings and calcium ions [40]. Because of its high symmetry, its (100), (010), (100), (200), (020) and (002) cleavage planes are equivalent, and also resulted in the lowest energy [99]. From MD simulations with IFF parameters for C_3A, values of 1.26 J/m^2 and 1.21 J/m^2 were calculated at 298 K and 363 K [99]. The latter corresponds to the typical temperature employed for clinker grinding. At 298 K, the system recovered about 70% of its initial energy after agglomeration, and 40% for superficially hydrated surfaces [99]. In comparison, a cleavage energy of 1.34 J/m^2 was reported for the (010), Ca-rich plane of M_3-C_3S, and recovered only 35% and 20% upon agglomeration of the dry and superficially hydrated surfaces, respectively [83]. In addition, these simulations provide insightful results on

Phase	Method	Surface energy ($J\,m^{-2}$)							Ref.
		(100)	(010)	(001)	(110)	(101)	(011)	(111)	
M_3-C_3S [89]	DFT, PAW, PBE	1.38	1.09	1.19	0.98	1.25	1.14	0.96	[87]
M_3-C_3S [89]	EM, ReaxFF	1.46	1.64	1.31	1.58	1.31	1.34	1.31	[82]
M_3-C_3S [90]	MD*, IFF	1.40(4)	1.32(3)	1.33(3)	–	1.38(4)	–	–	[83]
M_3-C_3S [90]	MD*, IFF	1.14(3)	1.31(4)	1.22(4)	1.36(5)	1.37(3)	1.34(5)	1.24(4)	[91, 92]
M_1-C_3S [93]	MD*, IFF	1.04(4)	1.41(4)	1.20(4)	1.45(4)	1.51(3)	1.17(4)	1.43(3)	[92]
T_1-C_3S [94]	DFT, PAW, PBE	1.17	1.23	1.22	1.28	1.50	1.15	1.20	[88]
β-C_2S [95]	DFT, PAW, PBE	0.67	0.78	0.8	0.98	0.95	0.83	0.95	[87]
β-C_2S [62]	DFT, PW, PBE	0.85	1.00	1.05	1.37	0.76	1.03	1.20	[39]
γ-C_2S [96]	DFT, PW, PBE	1.72	1.13	1.87	2.25	1.47	1.42	1.52	[39]
γ-C_2S [97]	DFT, PW, PBE+D2	–	1.27	–	–	–	–	–	[38]
C_3A [98]	MD, IFF	1.26	–	–	–	–	–	–	[99]

Table 1: Lowest surface energy computed in each direction for C_2S, C_3S and C_3A. *Series of temperature gradients on superficial ions were applied to reach more energetically favorable configurations. EM: Energy minimization. PW: Plane-wave basis sets. PAW: Projector augmented-wave method [100]. PBE: Perdew, Burke and Ernzerhof generalized gradient approximation (GGA) functional for the exchange-correlation energy [101]. D2: Grimme D2 correction for van der Waals interaction [102].

the effect of different molecules employed as dispersant in the clinker grinding process [83, 99].

The Wulff construction is based on the free energy minimization of surfaces and provides theoretical representation of crystal shapes. Several representation of M_3-C_3S were proposed in the literature based on surface and cleavage energy calculations [39, 82, 83, 87, 92] (see Fig. 2). More sharped edges of C_3S compared to C_2S, also observed on micrographs [103], were obtained from DFT calculations [87]. Furthermore, MD calculations with IFF resulted in a rounder shape for the M_1 polymorph than for M_3-C_3S [92]. Although thicker, the shape obtained for M_1-C_3S was similar to the equilibrium form proposed by Maki [47]. One should note that to provide a complete theoretical crystal, surface energies must be calculated for every possible cleavage plane. Furthermore, the Gibbs free minimization implies that surfaces with larger energies, presumably more reactive, have smaller area. Such surfaces might dissolve faster upon contact with water resulting in rounder crystal shapes and more homogeneous surfaces with equivalent dissolution kinetics. This means that surface energy could only indicates the tendency of a surface to react over very short timescale. Indeed, a reactive MD investigation demonstrated that the topological evolution of the surface during hydration resulted in similar water dissociation profiles after a few hundred picoseconds [82].

M_1-C_3S [93]			M_3-C_3S [90]			
Miller index	Shift*	Surface energy ($J\,m^{-2}$) [92]	Miller index	Shift*	Surface energy ($J\,m^{-2}$) [91, 92]	[83]
(100)	0.0774	1.09(4)				
(100)	0.25125	1.19(4)	(100)	–	1.39(3)	1.53(6)
(100)	0.3662	1.46(4)	(300)	–	1.14(3)	1.59(3)
(100)	0.4746	1.38(4)	(800)	–	1.17(3)	1.40(4)
(100)	0.586	1.04(4)	(010)	–	1.55(4)	1.33(4)
(100)	0.731	1.28(4)	(040)	–	1.31(4)	1.32(3)
(100)	0.932	1.16(4)	(001)	–	1.38(4)	1.33(3)
(100)	0.9658	1.18(4)	(002)	–	1.45(4)	1.35(4)
(010)	–	1.41(4)	(003)	–	1.31(4)	1.33(3)
(040)	–	1.76(3)	(00-3)	–	1.33(4)	1.33(3)
(003)	–	1.20(3)	(008)	–	1.22(4)	1.44(3)
(004)	–	1.49(4)	(00-8)	–	1.22(4)	1.44(3)
(008)	–	1.20(4)	(110)	0.44095	1.36(5)	–
(110)	0.01565	1.45(4)	(101)	0.28285	1.37(3)	–
(101)	0.02075	1.51(3)	(011)	0.26085	1.34(5)	–
(011)	0.02725	1.17(4)	(111)	0.4364	1.24(4)	–
(111)	0.76475	1.43(3)	(-10 0 3)	–	–	1.38(4)

Table 2: Surface energies of M_1 and M_3 C_3S computed for multiple planes in different direction. *Distance of the plane from the origin in lattice-plane spacing units.

3. Anhydrous clinker phases/water interfaces

3.1. Adsorption of single and a few water molecules at 0 K

Reactive sites of surfaces can be identified by simulating the adsorption of a single water molecule at different locations, finding the minimum energy configuration and calculating the adsorption energy. To ensure that the minimum energy configuration is reached, the initial distance of the water molecule should be optimized and several initial orientations should be simulated [39, 82]. DFT and reactive FF can describe reactions and thus the dissociation of water molecules on surfaces. Simulations with ReaxFF pointed out a lack of correlation between surface energies and average adsorption energies for various surfaces of M_3-C_3S [82]. Likewise, no correlation was found between surfaces energies and the percentage of area where water dissociation occurs. These observations indicate that surface energy is insufficient to conclude on the reactivity and that simulations of the adsorption of water molecules could provide more meaningful information.

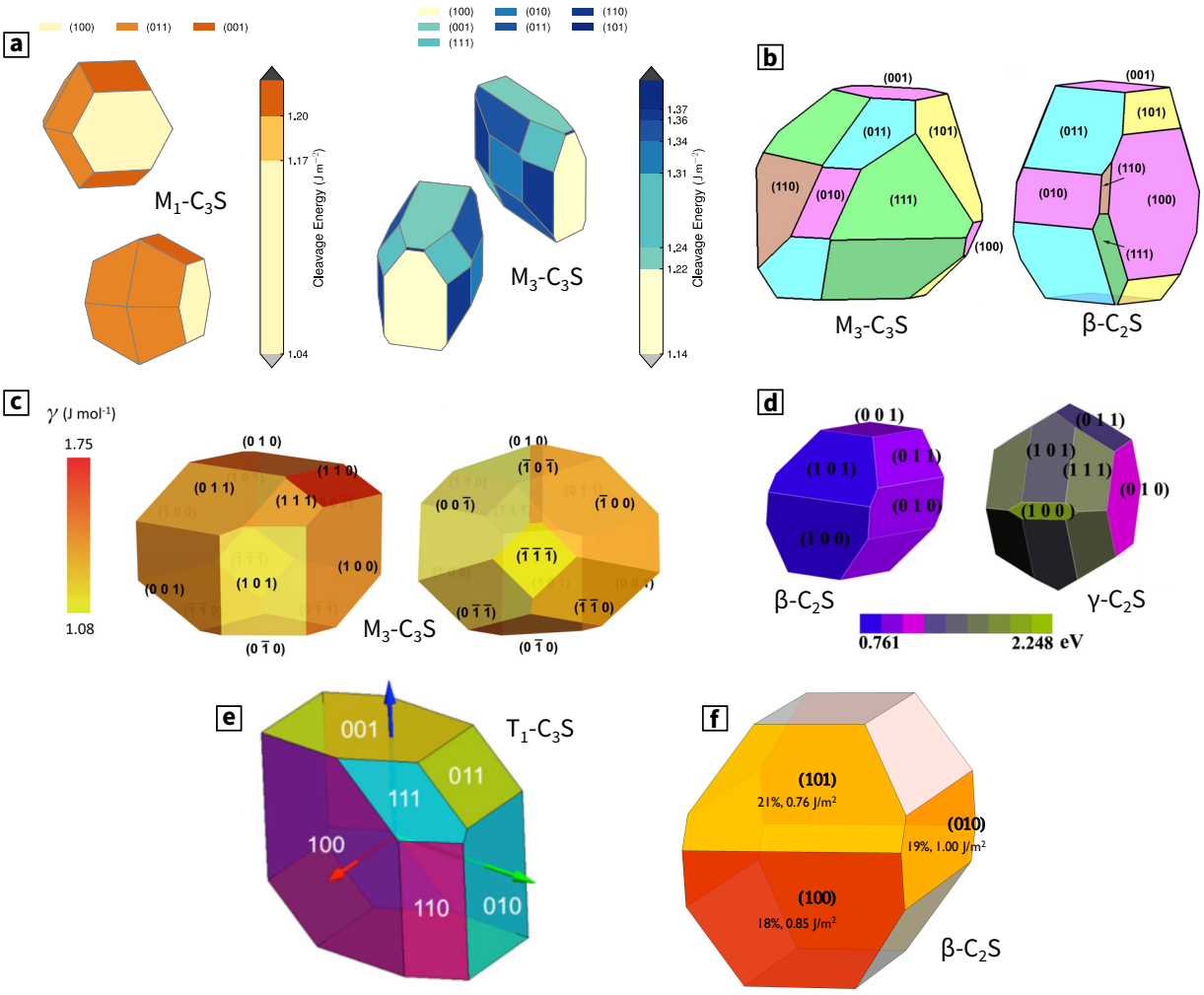

Figure 2: Wulff shapes of a) M_1-C_3S and M_3-C_3S [92], b) M_3-C_3S and β-C_2S [87], c) M_3-C_3S [82] d) M_3-C_3S and β-C_2S [39], e) T_1-C_3S [88], f) β-C_2S [86] (computed in [39]). The color scales indicate the surface or cleavage energy.

DFT investigations were carried out to depict the adsorption of single water molecules on M_3-C_3S surfaces [104–106]. In general, adsorption energies are larger (in absolute value) for dissociative adsorption than for molecular adsorption, suggesting a higher probability for the former to occur. Moreover, dissociative adsorption is – as expected – favoured by a closer initial distance between the water molecule and oxide anions. Although dissociative adsorption was also observed on oxygen atoms in orthosilicate ions. Indeed, Zhang et al. reported that the LDOS of the VBM, which is exclusively localized around Oi atoms in the bulk crystal, was also localized around Oc atoms on surfaces containing silicates, making them vulnerable to electrophilic attacks [104] (see Fig. 3). On a (111) surface, the same authors reported a decrease in adsorption energy with the number of adsorbed water molecules, due to the formation of H-bonds between

them [105]. The influence of Ca to Mg substitution on the water adsorption on M_3-C_3S and β-C_2S was also investigated [107]. For almost all the investigated surfaces, the formation energy of Mg impurities was energetically unfavorable and did not affect significantly the frequency of water dissociation.

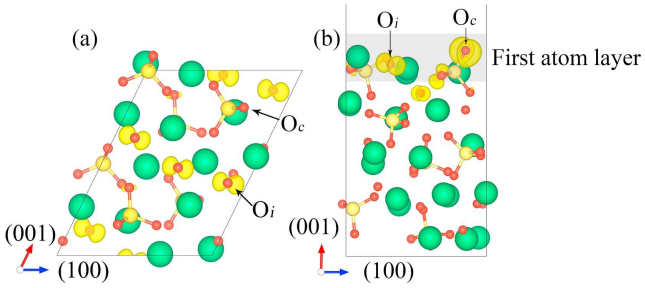

Figure 3: LDOS of the VBM a) bulk unit cell and b) (100) surface of M_3-C_3S. Color code for atoms: Ca in green, O in red, Si in yellow.

DFT calculations by Wang et al. resulted in smaller cleavage energies for β-C_2S than for γ-C_2S [39] (see Table 1). This may be a counterintuitive result since high-energy surfaces reveal instability and could be an indicator of reactivity. Nonetheless, adsorption simulations of single water molecule with ReaxFF indicated that despite higher adsorption energies, less reaction sites were found on γ-C_2S than on β-C_2S surfaces [39]. The adsorption energies on γ-C_2S surfaces were in excellent agreement with previous DFT calculations [38]. Moreover, simulations of C_2S surfaces in contact with a water film showed that less water dissociation occurs on the γ-C_2S(010) than on the β-C_2S(100) surface and that the reaction rate slow down earlier for the former. The authors suggested that the larger reactivity of β-C_2S compared to the γ polymorph may be due to its lower symmetry [39]. Simulations of water adsorption on different β-C_2S surfaces suggest a dual interaction of water with a C_2S surface including a nucleophilic interaction of the water oxygen lone pair with surface calcium atoms and an electrophilic interaction (hydrogen bond) of one water hydrogen with surface oxygen atoms [86]. A similar interaction pattern was reported for a water-C_3S interface [108]. However, no correlation was found between the electronic structure and the adsorption energies [86]. As reported for M_3-C_3S, DFT calculations on the β-C_2S (100) surface resulted in higher energies for dissociative adsorption than for molecular adsorption [109].

3.2. Interface with water film and surface protonation

Adsorption simulations of single water molecule by DFT or reactive FF may indicate the most reactive sites. However, this method presents several limitations: 1) energy minimization methods does not account for thermal fluctuations, which is an important factor for proton exchange in bulk water, and between water and a solid surface [108]. 2) interactions between water molecules which affect the adsorption energy are not considered. 3) the properties of bulk and interfacial water molecules cannot be described.

Classical MD simulations are suitable to study solid/liquid interfaces where the hydrogen bond (HB) network is responsible for the structural and dynamical behaviour of water. Analysis of trajectories can provide for example: atomic density profiles perpendicularly to a surface, preferential orientation and diffusion coefficient of water molecules as a function of the distance from the surface, or the lifetime of different HB. Classical MD cannot simulate reactive events but may give information on the probability of water dissociation and protonation at a specific site based on the lifetime of HB [91]. However, only reactive or ab initio MD (AIMD) are able to describe properly the evolution of the protonation states of a surface over time [82, 88, 108]. AIMD has a high level of theory because interatomic forces are calculated by quantum mechanics at each time step (for Born-Oppenheimer MD). The computational cost is much greater than for classical MD and the typical simulation time is about a few tenth of picoseconds. Conversely, reactive FF such as ReaxFF are less computationally expensive but require an optimization of specific parameters for the system under study.

At the vicinity of a solid surface, water molecules are found in a particular arrangement known as HB network, which is influenced by the substrate structure, composition, and charge distribution [110]. AIMD simulations of the M_3-C_3S(010)/water interface pointed out a three-layered water structure within ∼5–6 Å (see Fig. 4), where two regions coexist: one calcium-rich, and the other silicate-rich [108]. Interestingly, water molecules of the first layer (at <2 Å from the surface) adopted two preferential orientation corresponding to these two regions. In the calcium-rich region, water molecules formed a bond between their oxygen atom and calcium cations. This resulted in an angle θ between their dipole moment and the outward-pointing normal to the surface of 120 to 160°. In the other region, water molecules formed two HB with orthosilicate ions ${SiO_4}^{4-}$ (θ from 20 to 50°). In the silicate-rich region, some water molecules also arranged with their dipole moment parallel to the surface ($\theta \sim 90°$). This configuration corresponds to water molecules forming one HB with ${SiO_4}^{4-}$. All these configurations were also reported in DFT simulation of water adsorption on olivine surfaces [38]. One should note that since the configuration of water molecules in the first layer is directly dependent of the surface topology, the construction of the atomistic model plays an important role in the result. Furthermore, the HB network is likely to evolve with increasing water coverage, which should be high enough to reproduce properly the behaviour of an interface with mixing water.

The parametrization of a Ca/Si/O/H set for ReaxFF made possible the simulation of M_3-C_3S/water interfaces for multiple surfaces [82]. The systems were simulated for 2 ns and most of the water dissociation occurred during the first 0.3 ns. After this first hydration step, the reaction rate decreased and a decelerated regime was reached. With the same FF, similar results were reported for T_1-C_3S surfaces doped with Mg, Al and Fe [88]. Manzano et al. reported a tesselation process on the (001)M_3-C_3S surface, where the hydration stabilizes after the initial protonation of the surface [82]. For the other surfaces, a proton hopping

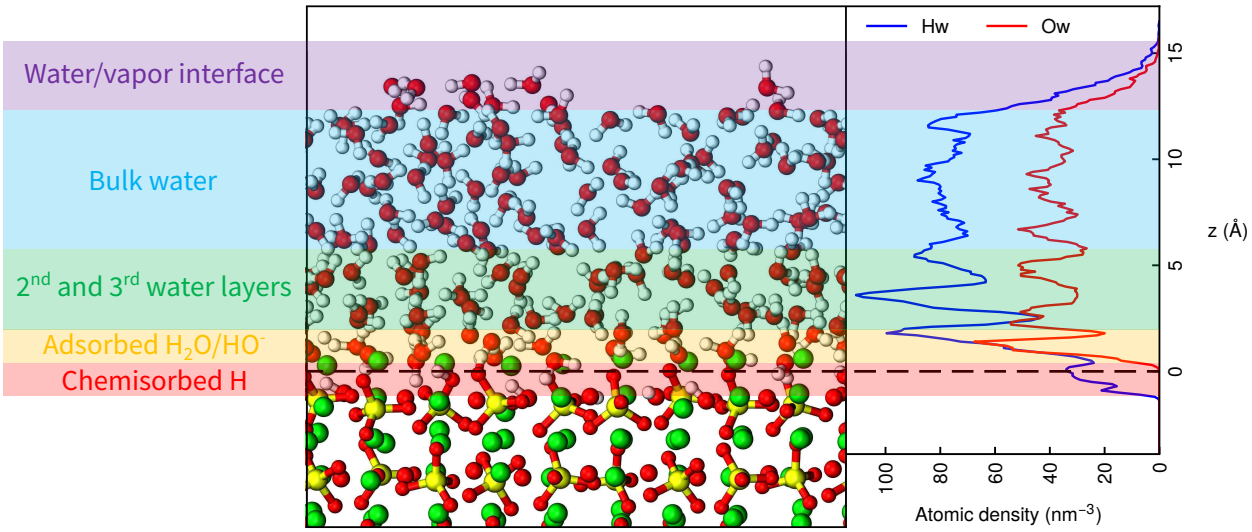

Figure 4: Snapshot and atomic density of a water film on a M_3-C_3S (010) surface. Color code for atoms: Ca in green, O in red, Si in yellow, H in white. Adapted from [108].

mechanism from a superficial hydroxide to inner oxygen atoms was reported and depicted in Fig. 5. The diffusion of protons inside the bulk induced a desorption of calcium atoms and a rearrangement of silicate tetrahedrons, which may lead to their oligomerization. It was also pointed out that the surface energy only influenced the reaction rate during the first hydration step, after which the water dissociation evolved at the same rate for every plane (except (100)) due to the loss of crystallinity [82]. Such observation also strengthens the idea that surface energy itself cannot provide enough information on reactivity.

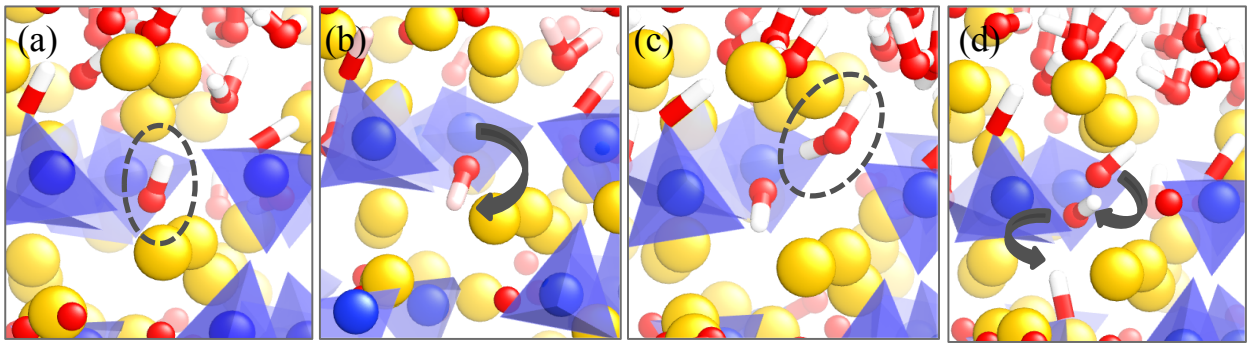

Figure 5: Snapshot of the proton hopping mechanism on a M_3-C_3S (010) surface a) a water molecule dissociate and protonate an oxide ion on the surface. b) the superficial hydroxide ion rotates due to the thermal vibration. c) a water molecule forms a HB with of the hydroxide ion. d) a proton hopping occurs from the water molecule to the hydroxide ion, and from the hydroxide ion to an inner oxygen atom. Color code for atoms: Ca in green, H in white, O in red (except Oc atoms), Si atoms and silicate tetrahedrons are in blue. Reprinted with permission from [82]. Copyright 2015 American Chemical Society.

Recently, an AIMD simulation on a (010), calcium rich M_3-C_3S surface was compared with a ReaxFF simulation during 18 ps. Three type of hydroxyl groups were considered: hydroxyls in silanol H-Oc, hydroxyls formed on oxide ions H-Oi, and hydroxyls resulting from water dissociation H-Odw. The evolution of the different hydroxyl groups showed a very good agreement between the AIMD and the ReaxFF simulation. However, in the AIMD simulation, a fluctuation of the number of H-Oc and H-Odw groups was observed as a consequence of back and forth proton transfer (PT) in contrast with ReaxFF simulations where the number of hydroxyl groups stabilized very quickly within the simulation time [108]. In both simulations, and as expected, hydroxides formed on oxide ions were very stable and did not involve PT after the first protonation. However, only Oi at specific sites were protonated, while the protonation at other sites was hindered by calcium cations. The free energy was calculated for PT between water molecules and orthosilicate ions, and between water molecules and superficial hydroxides formed upon water dissociation. Analysis of free energy maps pointed out the instability of silanol groups over the simulation time that may be too short to reproduce the preponderance of protonated silicates at the surface of C_3S, revealed by NMR measurements [111]. Likewise, the molecular form of water on the surface was found to be more stable than hydroxides. This result seems contradictory with DFT investigation on the adsorption of single water molecules, suggesting a higher probability of dissociative adsorption [104]. Such discrepancy has two explanations: the difference in the number of water molecules used in both models, thus including interactions amongst them, and the consideration of thermal fluctuations in the AIMD simulation against a static representation in the DFT studies. This point out the relevance of a model with a water film simulated at finite temperature, thus describing the fluctuation of the HB network which plays a key role in PT [108, 112]. Another important result from this study is that the typical lifetime of PT between water and Oc and between water and Odw was ~ 20 fs. Interconversion events between Eigen and Zundel ions in bulk water were measured experimentally on the same timescale (< 100 fs) [113]. Similar lifetime was obtained for PT at water/ZnO interface [112]. This suggests that the PT frequency on a C_3S surface at the very early stage of the hydration is controlled by the PT that occurs in bulk water.

The hydration process can be seen as a sequence of system states at different time. Applying this reasoning, Pustovgar et. al proposed parameters for IFF to model the hydration of a C_3S surface [114] incrementally. The proposed protonation states were related to the pK of silicic acid and to the pH. Based on this model, the influence of $NaAlO_2$ and the hindering of C_3S hydration by aluminate was investigated. MD simulations suggested that adsorption of aluminate ions occurs only for pH < 13. However, covalent bonds that should be formed in silicate-aluminate complexes were not detected by NMR [114]. The same hydration model was employed to assess the behaviour of water at the interface with a (010) surface of M_3-C_3S for different hydration degree [91] (see Fig. 6). Before any protonation occurs, some water molecules in contact with the surface formed two strong HB with Oi and Oc. These water molecules kept fixed to the

surface and constituted a base for the structured HB network depicted in atomic density profiles [91]. With increasing protonation degree, this network decayed and the rotational and translational motion of water molecules increased. The same strong interaction and reduced mobility of water molecules at the vicinity of an anhydrous C_3S surface were reported using ClayFF [115]. In the presence of sodium and sulfate ions, the authors observed the formation of a ionic layer inhibiting the dissolution. Another study pointed out the effect of surface dissimilarity on the structural and dynamic properties was pointed out for water films confined between C_3S-C_3S, C_2S-C_2S and C_3S-C_2S anhydrous surfaces [116].

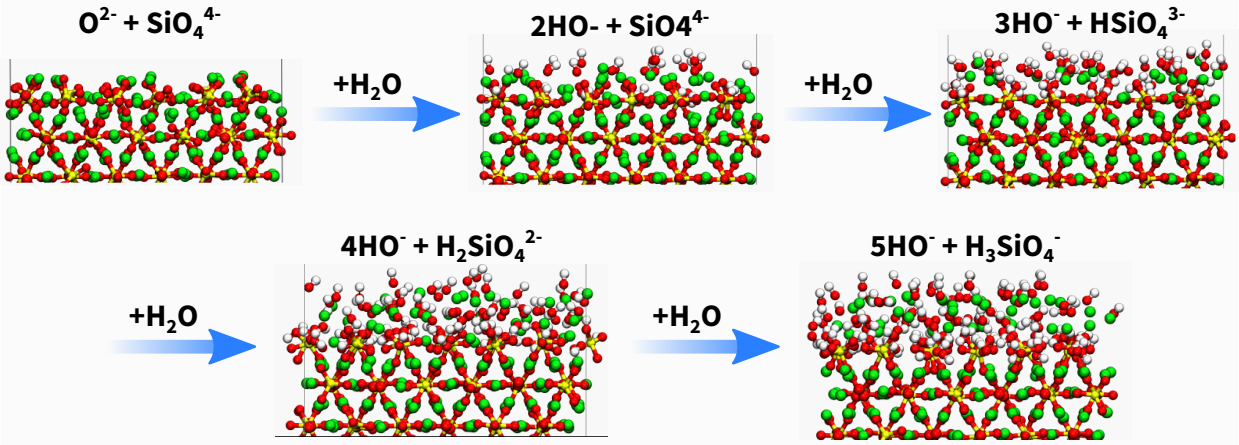

Figure 6: Relaxed surface for different hydration degree of a M_3-C_3S (010) surface [91], applying the hydration model proposed by Pustovgar et al. [114]. Color code for atoms: Ca in green, O in red, Si in yellow, H in white.

It is not straightforward to make a link between water/clinker phases simulations at the atomic scale and hydration curves from calorimetry measurements. Classical MD simulations can only describe the arrangement of water molecules on the surface and the lifetime of bonds, which may indicate what reactions should occur at first. Reactive MD can describe the triggering and mechanisms of the very early hydration. In both cases, the principal limitation is the timescale. It is known that due to the humidity of the environment, C_3S experience a superficial hydration even before the addition of water leading to a decrease in surface energy [5, 117]. As a consequence, a delayed hydration for samples of clinker phases exposed to controlled humidity was reported from calorimetry and X-ray photoelectron spectroscopy (XPS) measurements [118]. NMR measurements can provide insights on the kinetics of silicate polymerization which occurs during the acceleration and deceleration periods [111]. ^{29}Si and $^{1}H\{^{29}Si\}$ cross-polarization magic-angle-spinning NMR measurements also revealed the presence of hydroxylated silicate monomers even before contact with bulk water [111]. To this end, the above mentioned new version of the IFF parameters for C_3S, taking into account the hydroxylation of superficial silicates, was developed [114]. However, negligible silicate polymerization was reported in C_3S in contact with atmospheric moisture [111]. Nonetheless, XPS analysis of thin films of clinker phases prepared by electron beam evaporation and hydrated under saturated water

vapor pressure evidenced a shift to higher binding energies on Si-2p photoelectron spectra, related to silicate polymerization [119–123]. Ambient pressure X-ray photoelectron spectroscopy (APXPS) allowed to quantify the water coverage and composition of the hydration layer (number of oxide ions, oxygen in hydroxyls and molecular water) based on the shift in binding energy of O-1s spectra with increasing vapor pressure [124]. This method was employed for oxides such as MgO [125, 126], Al_2O_3 [127], CaO [126, 128] and SiO_2 [129] and α-Fe_2O_3 [130]. Such measurements require a particular effort for the preparation of samples and the prevention from pre-hydration, carbonation and contaminants. Furthermore, the preparation of a specific surface is feasible for metals and simple oxides but would be technically challenging for clinker phases. The morphology of surface at the atomic scale can be assessed by atomic force microscopy (AFM) and scanning tunneling microscopy (STM). STM observations indicated a disorder of the CaO(001), hydroxylated surface for a water coverage of about one monolayer [128]. Such disorder was also verified by reactive MD simulations [24]. Moreover, the difference in hydration layer structure of dolomite, calcite and magnesite were outlined by MD simulations, by extracting the water density along specific sites [131] or by explicitly modeling a silicon AFM tip [132]. These simulations were found to be in remarkable agreement with experimental AFM measurements.

4. Limitations and perspectives

Previous studies clearly demonstrated that a lack of information arises from electronic structure assessment of bulk crystals, thus justifying the need of surface modeling to identify the most reactive regions [82, 104]. However, the surface energy itself has shown to be insufficient to conclude on reactivity [39, 82]. The mapping of adsorption energy and dissociation points seems to be more appropriated but does not account for thermal fluctuation which induces topological changes, lowers energy barriers and enhances proton mobility [39, 82, 86]. Among the different methods reviewed herein, MD simulations of water films in contact with a surface may be the most appropriate method to account for the different mechanisms actually occurring at solid/liquid interface [82, 108, 112]. A strong limitation of classical FF in comparison with reactive FF is their inability to describe bond forming and breaking, reducing the description to a specific chemical environment for each atom type. Nonetheless, a classical description of C_3S surfaces for different degree of hydration was proposed, starting from the protonation of oxide ions before the incremental protonation of silicates [83, 114]. However, an AIMD investigation revealed that the hydroxylation of superficial Oi atoms depends on their position and may be hindered by the presence of calcium ions in its vicinity [108]. In this simulation, despite the lower pKa of silicic acid compared to hydroxide resulting in weaker H-Oc bonds than H-Oi bonds, some Oc atoms were protonated before Oi atoms. The delocalization of reactive regions from Oi in bulk C_3S to Oc at C_3S surfaces also strengthens this idea [104]. From a deterministic point of view, the difference in protonation state at the very beginning of the hydration – even before contact with liquid

water – may influence the rearrangement of superficial species and further hydration mechanisms. Reactive MD simulations successfully described the evolution of the hydration of surfaces over a few nanoseconds and suggested that their dissimilarity influenced the hydration regime only during a few hundreds of picoseconds [82, 88]. After the initial, rapid hydration step, the hydration rates of the different surfaces decreased and homogenized because of the similar topologies of surfaces that have lost their crystalline arrangement [82]. A relevant question is: to what extent the surface structure and initial protonation state – related to the exposure to humidity – will influence the hydration mechanisms and kinetics at an experimentally observable scale? Traditional MD is currently limited by the computational cost, making impossible the simulation of hydration at this scale. However, some alternative methods could overcome this limitation.

A first solution consists in simulating systems at high temperature to increase the hydration reaction rate. The latter can be assessed by linear fitting of the number of reacted water molecules as a function of time within the decelerated hydration step (after few hundreds of ps). Based on transition state theory (TST), the Arrhenius equation relates the activation energy with the reaction rate as a function of the temperature. Applying this relation, ReaxFF simulations of M_3-C_3S interfaces at temperatures between 800 and 1600 K resulted in activation energies between 25.7 kJ/mol and 39.1 kJ/mol for different surfaces [133]. In comparison, values of 13–26 kJ/mol and 49 kJ/mol were found far from, and close to equilibrium respectively, by dissolution measurements in cell [7].

Kinetic Monte Carlo (KMC) is based on TST and, contrary to MD, do not aim to capture the entire dynamical evolution of the system, but consider events – or transitions from one state to another – occurring with different probability over time. Since only specific events are considered, KMC simulations generally require less computational power and can predict the evolution of a surface for longer hydration period. A Kossel crystal or terrace ledge kink (TLK) model consists in a structure of elementary cubes attached by their faces. A cube can have up to six nearest neighbors, which is the case in the bulk. The surface is formed by cubes with five or less nearest neighbors and can contains dislocations (see Fig. 7a). Recent studies considering dissociation and precipitation rates on Kossel crystals reproduced the experimentally observed sigmoidal dependence between the dissolution rate and the Gibbs free energy for several minerals including alite (see Fig. 7b) [134, 135]. In a more recent study, the dissolution of alite under different hydrodynamic conditions was considered employing the same KMC coupled with Lattice Boltzmann models to simulate a fluid flow and the transport of ions [136]. Moreover, off-lattice KMC simulations predicted the effect of screw dislocations on the mechanisms and rates of dissolution C_3S [137]. The precipitation of C-S-H nanoparticles on a substrate was also investigated with a similar method using parameters from experiments and previous nanoscale modeling of C-S-H [138]. Substrates with favorable nucleation sites led to precipitation rates in good agreement with the boundary nucleation and growth mechanism, also known

as Cahn mechanism.

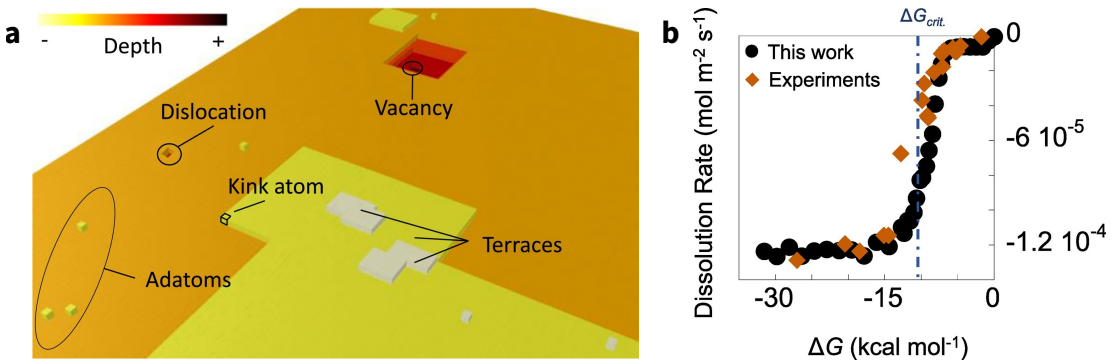

Figure 7: a) Topographic defects on a Kossel crystal surface. b) Simulated [134] (in black) and experimental [139] (in orange) dissolution rate as a function of the Gibbs free energy for alite at 300 K.

The parallel tempering method consists in running several simulations at different temperatures and performing swap moves between systems with adjacent temperatures [140]. At high temperature, more states can be sampled, the probability for a rare event to occurs is thus greater than at lower temperature. Swaps between systems allow low-temperature systems to escape local energy minima and to explore larger regions of the phase space. In recent studies, parallel tempering simulations of silicate in pure water and NaOH solutions allowed to accelerate the gelation process by several orders of magnitude compared to MD and showed good agreement with experimental measurements [141, 142]. To our knowledge, no parallel tempering simulation of liquid/mineral interface has been reported so far.

5. Conclusions

In recent years, DFT calculations have improved our understanding on the origins of the reactivity of the principal PC clinker phases based on their electronic structure. Additionally, several studies assessed the enthalpy of formation of substitutional defects and their influence on the electronic structure in bulk crystal. However, no pathway to a significant enhancement of reactivity induced by doping was provided. It was demonstrated that the electronic structure differs significantly from bulk crystals to surfaces, and that the very early hydration is driven by the surface properties. However, a reactive MD study suggested that such properties only affect the hydration kinetics during a first, rapid step after which the dissociation of water molecules follows a slow regime that is very similar for different surfaces. Yet it is probable that the topological features of the surface may impact the dissolution mechanisms at longer timescales. Several simulation methods that could solve the timescale issue were reviewed. In particular, KMC simulations

provided insights on the mechanisms of precipitation of C-S-H nanoparticles on a substrate, and on the dissolution of alite from a simplistic model as a Kossel crystal. This is a very promising method that can consider dislocations and the formation of etch pits, whose nucleation, expansion and coalescence could drive the dissolution rate of alite [4]. To go further in the description of dissolution mechanisms, more realistic crystal models that consider ions explicitly could be employed. To this end, dissociation energy barriers of ions with different environments could be calculated from atomistic simulations. The hydration of Portland cement involve many mechanisms of dissolution, diffusion and precipitation that are closely related. Towards a more accurate description, a huge challenge remains in the implementation of models that could describe these mechanisms concurrently.

Acknowledgements

Qianqian Wang would like to thank the National Natural Science Foundation of China (Nanjing, Grant number: 52072171) for funding this research.

References

[1] K. L. Scrivener, A. Nonat, Hydration of cementitious materials, present and future, Cement and Concrete Research 41 (7) (2011) 651–665. doi:10.1016/j.cemconres.2011.03.026.

[2] K. Scrivener, A. Ouzia, P. Juilland, A. K. Mohamed, Advances in understanding cement hydration mechanisms, Cement and Concrete Research 124 (2019) 105823. doi:10.1016/j.cemconres.2019.105823.

[3] J. W. Bullard, H. M. Jennings, R. A. Livingston, A. Nonat, G. W. Scherer, J. S. Schweitzer, K. L. Scrivener, J. J. Thomas, Mechanisms of cement hydration, Cement and Concrete Research 41 (12) (2011) 1208–1223. doi:10.1016/j.cemconres.2010.09.011.

[4] P. Juilland, L. Nicoleau, R. S. Arvidson, E. Gallucci, Advances in dissolution understanding and their implications for cement hydration, RILEM Technical Letters 2 (2017) 90. doi:10.21809/rilemtechlett.2017.47.

[5] P. Juilland, E. Gallucci, R. Flatt, K. Scrivener, Dissolution theory applied to the induction period in alite hydration, Cement and Concrete Research 40 (6) (2010) 831–844. doi:10.1016/j.cemconres.2010.01.012.

[6] L. Nicoleau, A. Nonat, A new view on the kinetics of tricalcium silicate hydration, Cement and Concrete Research 86 (2016) 1–11. doi:10.1016/j.cemconres.2016.04.009.

[7] P. Juilland, E. Gallucci, Morpho-topological investigation of the mechanisms and kinetic regimes of alite dissolution, Cement and Concrete Research 76 (2015) 180–191. doi:10.1016/j.cemconres.2015.06.001.

[8] A. Kumar, B. J. Walder, A. K. Mohamed, A. Hofstetter, B. Srinivasan, A. J. Rossini, K. Scrivener, L. Emsley, P. Bowen, The Atomic-Level Structure of Cementitious Calcium Silicate Hydrate, The Journal of Physical Chemistry C 121 (32) (2017) 17188–17196. doi:10.1021/acs.jpcc.7b02439.

[9] N. Krautwurst, L. Nicoleau, M. Dietzsch, I. Lieberwirth, C. Labbez, A. Fernandez-Martinez, A. E. S. V. Driessche, B. Barton, S. Leukel, W. Tremel, Two-Step Nucleation Process of Calcium Silicate Hydrate, the Nanobrick of Cement, Chemistry of Materials (apr 2018). doi:10.1021/acs.chemmater.7b04245.

[10] P. Hohenberg, W. Kohn, Inhomogeneous Electron Gas, Physical Review 136 (3B) (1964) B864–B871. doi:10.1103/physrev.136.b864.

[11] W. Kohn, L. J. Sham, Self-Consistent Equations Including Exchange and Correlation Effects, Physical Review 140 (4A) (1965) A1133–A1138. doi:10.1103/physrev.140.a1133.

[12] R. K. Mishra, A. K. Mohamed, D. Geissbühler, H. Manzano, T. Jamil, R. Shahsavari, A. G. Kalinichev, S. Galmarini, L. Tao, H. Heinz, R. Pellenq, A. C. van Duin, S. C. Parker, R. J. Flatt, P. Bowen, cemff : A force field database for cementitious materials including validations, applications and opportunities, Cement and Concrete Research 102 (2017) 68–89. doi:10.1016/j.cemconres.2017.09.003.

[13] R. T. Cygan, J.-J. Liang, A. G. Kalinichev, Molecular Models of Hydroxide, Oxyhydroxide, and Clay Phases and the Development of a General Force Field, The Journal of Physical Chemistry B 108 (4) (2004) 1255–1266. doi:10.1021/jp0363287.

[14] R. T. Cygan, J. A. Greathouse, A. G. Kalinichev, Advances in Clayff Molecular Simulation of Layered and Nanoporous Materials and Their Aqueous Interfaces, The Journal of Physical Chemistry C (jul 2021). doi:10.1021/acs.jpcc.1c04600.

[15] R. Shahsavari, R. J.-M. Pellenq, F.-J. Ulm, Empirical force fields for complex hydrated calcio-silicate layered materials, Physical Chemistry Chemical Physics 13 (3) (2011) 1002–1011. doi:10.1039/c0cp00516a.

[16] G. V. Lewis, C. R. A. Catlow, Potential models for ionic oxides, Journal of Physics C: Solid State Physics 18 (6) (1985) 1149–1161. doi:10.1088/0022-3719/18/6/010.
URL https://doi.org/10.1088/0022-3719/18/6/010

[17] K.-P. Schröder, J. Sauer, M. Leslie, C. Richard, A. Catlow, J. M. Thomas, Bridging hydrodyl groups in zeolitic catalysts: a computer simulation of their structure, vibrational properties and acidity in protonated faujasites (HY zeolites), Chemical Physics Letters 188 (3-4) (1992) 320–325. doi:10.1016/0009-2614(92)90030-q.

[18] C. L. Freeman, J. H. Harding, D. J. Cooke, J. A. Elliott, J. S. Lardge, D. M. Duffy, New Forcefields for Modeling Biomineralization Processes, The Journal of Physical Chemistry C 111 (32) (2007) 11943–11951. doi:10.1021/jp071887p.

[19] G. W. Watson, E. T. Kelsey, N. H. de Leeuw, D. J. Harris, S. C. Parker, Atomistic simulation of dislocations, surfaces and interfaces in MgO, Journal of the Chemical Society, Faraday Transactions 92 (3) (1996) 433. doi:10.1039/ft9969200433.

[20] N. H. Leeuw, S. C. Parker, Effect of Chemisorption and Physisorption of Water on the Surface Structure and Stability of alpha-Alumina, Journal of the American Ceramic Society 82 (11) (2004) 3209–2316. doi:10.1111/j.1151-2916.1999.tb02225.x.

[21] H. Heinz, T.-J. Lin, R. K. Mishra, F. S. Emami, Thermodynamically Consistent Force Fields for the Assembly of Inorganic, Organic, and Biological Nanostructures: The INTERFACE Force Field, Langmuir 29 (6) (2013) 1754–1765. doi:10.1021/la3038846.

[22] A. C. T. van Duin, S. Dasgupta, F. Lorant, W. A. Goddard, ReaxFF: A Reactive Force Field for Hydrocarbons, The Journal of Physical Chemistry A 105 (41) (2001) 9396–9409. doi:10.1021/jp004368u.

[23] T. P. Senftle, S. Hong, M. M. Islam, S. B. Kylasa, Y. Zheng, Y. K. Shin, C. Junkermeier, R. Engel-Herbert, M. J. Janik, H. M. Aktulga, T. Verstraelen, A. Grama, A. C. T. van Duin, The ReaxFF reactive force-field: development, applications and future directions, npj Computational Materials 2 (2016). doi:10.1038/npjcompumats.2015.11.

[24] H. Manzano, R. J. M. Pellenq, F.-J. Ulm, M. J. Buehler, A. C. T. van Duin, Hydration of Calcium Oxide Surface Predicted by Reactive Force Field Molecular Dynamics, Langmuir 28 (9) (2012) 4187–4197. doi:10.1021/la204338m.

[25] J. C. Fogarty, H. M. Aktulga, A. Y. Grama, A. C. T. van Duin, S. A. Pandit, A reactive molecular dynamics simulation of the silica-water interface, The Journal of Chemical Physics 132 (17) (2010) 174704. doi:10.1063/1.3407433.

[26] H. Manzano, S. Moeini, F. Marinelli, A. C. T. van Duin, F.-J. Ulm, R. J.-M. Pellenq, Confined Water Dissociation in Microporous Defective Silicates: Mechanism, Dipole Distribution, and Impact on Substrate Properties, Journal of the American Chemical Society 134 (4) (2012) 2208–2215. doi:10.1021/ja209152n.

[27] S. Kerisit, S. C. Parker, J. H. Harding, Atomistic Simulation of the Dissociative Adsorption of Water on Calcite Surfaces,

The Journal of Physical Chemistry B 107 (31) (2003) 7676–7682. doi:10.1021/jp034201b.

[28] S. Kerisit, S. C. Parker, Free Energy of Adsorption of Water and Metal Ions on the $\{10\bar{1}4\}$ Calcite Surface, Journal of the American Chemical Society 126 (32) (2004) 10152–10161. doi:10.1021/ja0487776.

[29] S. Kerisit, D. J. Cooke, D. Spagnoli, S. C. Parker, Molecular dynamics simulations of the interactions between water and inorganic solids, Journal of Materials Chemistry 15 (14) (2005) 1454. doi:10.1039/b415633c.

[30] P. Fenter, S. Kerisit, P. Raiteri, J. D. Gale, Is the Calcite–Water Interface Understood? Direct Comparisons of Molecular Dynamics Simulations with Specular X-ray Reflectivity Data, The Journal of Physical Chemistry C 117 (10) (2013) 5028–5042. doi:10.1021/jp310943s.

[31] M. Wolthers, D. D. Tommaso, Z. Du, N. H. de Leeuw, Calcite surface structure and reactivity: molecular dynamics simulations and macroscopic surface modelling of the calcite–water interface, Physical Chemistry Chemical Physics 14 (43) (2012) 15145. doi:10.1039/c2cp42290e.

[32] M. Wolthers, D. D. Tommaso, Z. Du, N. H. de Leeuw, Variations in calcite growth kinetics with surface topography: molecular dynamics simulations and process-based growth kinetics modelling, CrystEngComm 15 (27) (2013) 5506. doi:10.1039/c3ce40249e.

[33] P. Raiteri, J. D. Gale, D. Quigley, P. M. Rodger, Derivation of an Accurate Force-Field for Simulating the Growth of Calcium Carbonate from Aqueous Solution: A New Model for the Calcite-Water Interface, The Journal of Physical Chemistry C 114 (13) (2010) 5997–6010. doi:10.1021/jp910977a.

[34] P. V. Cuong, B. Kvamme, T. Kuznetsova, B. Jensen, Molecular dynamics study of calcite, hydrate and the temperature effect on CO2transport and adsorption stability in geological formations, Molecular Physics 110 (11-12) (2012) 1097–1106. doi:10.1080/00268976.2012.679629.

[35] J. D. Gale, P. Raiteri, A. C. T. van Duin, A reactive force field for aqueous-calcium carbonate systems, Physical Chemistry Chemical Physics 13 (37) (2011) 16666. doi:10.1039/c1cp21034c.

[36] R. K. Mishra, K. Kanhaiya, J. J. Winetrout, R. J. Flatt, H. Heinz, Force field for calcium sulfate minerals to predict structural, hydration, and interfacial properties, Cement and Concrete Research 139 (2021) 106262. doi:10.1016/j.cemconres.2020.106262.

[37] J. C. C. Santos, F. R. Negreiros, L. S. Pedroza, G. M. Dalpian, P. B. Miranda, Interaction of Water with the Gypsum (010) Surface: Structure and Dynamics from Nonlinear Vibrational Spectroscopy and Ab Initio Molecular Dynamics, Journal of the American Chemical Society 140 (49) (2018) 17141–17152. doi:10.1021/jacs.8b09907.

[38] S. Kerisit, E. J. Bylaska, A. R. Felmy, Water and carbon dioxide adsorption at olivine surfaces, Chemical Geology 359 (2013) 81–89. doi:10.1016/j.chemgeo.2013.10.004.

[39] Q. Wang, H. Manzano, Y. Guo, I. Lopez-Arbeloa, X. Shen, Hydration Mechanism of Reactive and Passive Dicalcium Silicate Polymorphs from Molecular Simulations, The Journal of Physical Chemistry C 119 (34) (2015) 19869–19875. doi:10.1021/acs.jpcc.5b05257.

[40] H. F. W. Taylor, Cement Chemistry, Second Edition, Thomas Telford Ltd, 1997.

[41] M. Bigaré, A. Guinier, C. Mazières, M. Regourd, N. Yannaquis, W. Eysel, T. Hanh, E. Woermann, Polymorphism of Tricalcium Silicate and Its Solid Solutions, Journal of the American Ceramic Society 50 (11) (1967) 609–619. doi:10.1111/j.1151-2916.1967.tb15009.x.

[42] I. Maki, S. Chromý, Microscopic study on the polymorphism of Ca3SiO5, Cement and Concrete Research 8 (4) (1978) 407–414. doi:10.1016/0008-8846(78)90020-0.

[43] J. Plank, On the correct chemical nomenclature of C3S, tricalcium oxy silicate 130 (2020) 105957. doi:10.1016/j.cemconres.2019.105957.

[44] T. Staněk, P. Sulovský, The influence of the alite polymorphism on the strength of the Portland cement, Cement and Concrete Research 32 (7) (2002) 1169–1175. doi:10.1016/s0008-8846(02)00756-1.

[45] H. Zhou, X. Gu, J. Sun, Z. Yu, H. Huang, Q. Wang, X. Shen, Research on the formation of M1-type alite doped with MgO and SO 3 —A route to improve the quality of cement clinker with a high content of MgO, Construction and Building Materials 182 (2018) 156–166. doi:10.1016/j.conbuildmat.2018.06.078.

[46] I. Maki, K. Kato, Phase identification of alite in portland cement clinker, Cement and Concrete Research 12 (1) (1982) 93–100. doi:10.1016/0008-8846(82)90103-x.

[47] I. Maki, Relationship of processing parameters to clinker properties; influence of minor components, in: Proceedings of the 8th International Congress on the Chemistry of Cement, Vol. 1, 1986, pp. 34–47.

[48] W. V. Fernandes, S. M. Torres, C. A. Kirk, A. F. Leal, M. R. L. Filho, D. Diniz, Incorporation of minor constituents into Portland cement tricalcium silicate: Bond valence assessment of the alite M1 polymorph crystal structure using synchrotron XRPD data, Cement and Concrete Research 136 (2020) 106125. doi:10.1016/j.cemconres.2020.106125.

[49] Y. Gao, Z. Li, J. Zhang, Q. Zhang, Y. Wang, Synergistic use of industrial solid wastes to prepare belite-rich sulphoaluminate cement and its feasibility use in repairing materials, Construction and Building Materials 264 (2020) 120201. doi:10.1016/j.conbuildmat.2020.120201.

[50] G. Jing, J. Zhang, X. Lu, J. Xu, Y. Gao, S. Wang, X. Cheng, Z. Ye, Comprehensive evaluation of formation kinetics in preparation of ternesite from different polymorphs of Ca2SiO4, Journal of Solid State Chemistry 292 (2020) 121725. doi:10.1016/j.jssc.2020.121725.

[51] F. P. Glasser, L. Zhang, High-performance cement matrices based on calcium sulfoaluminate–belite compositions, Cement and Concrete Research 31 (12) (2001) 1881–1886. doi:10.1016/s0008-8846(01)00649-4.

[52] M. T. Pedersen, F. Jensen, J. Skibsted, Structural Investigation of Ye'elimite, Ca4Al6O12SO4, by 27Al MAS and MQMAS NMR at Different Magnetic Fields, The Journal of Physical Chemistry C 122 (22) (2018) 12077–12089. doi:10.1021/acs.jpcc.8b02497.

[53] A. Cuesta, A. Ayuela, M. A. G. Aranda, Belite cements and their activation, Cement and Concrete Research 140 (2021) 106319. doi:10.1016/j.cemconres.2020.106319.

[54] T. Link, F. Bellmann, H. M. Ludwig, M. B. Haha, Reactivity and phase composition of Ca 2 SiO 4 binders made by annealing of alpha-dicalcium silicate hydrate, Cement and Concrete Research 67 (2015) 131–137. doi:10.1016/j.cemconres.2014.08.009.

[55] J. Li, G. Geng, W. Zhang, Y.-S. Yu, D. A. Shapiro, P. J. M. Monteiro, The Hydration of β- and α/H-Dicalcium Silicates: An X-ray Spectromicroscopic Study, ACS Sustainable Chemistry & Engineering 7 (2) (2018) 2316–2326. doi:10.1021/acssuschemeng.8b05060.

[56] E. Durgun, H. Manzano, R. J. M. Pellenq, J. C. Grossman, Understanding and Controlling the Reactivity of the Calcium Silicate phases from First Principles, Chemistry of Materials 24 (7) (2012) 1262–1267. doi:10.1021/cm203127m.

[57] M. Laanaiya, A. Bouibes, A. Zaoui, Understanding why Alite is responsible of the main mechanical characteristics in Portland cement, Cement and Concrete Research 126 (2019) 105916. doi:10.1016/j.cemconres.2019.105916.

[58] R. G. Parr, W. Yang, Density functional approach to the frontier-electron theory of chemical reactivity, Journal of the American Chemical Society 106 (14) (1984) 4049–4050. doi:10.1021/ja00326a036.

[59] P. W. Ayers, M. Levy, Perspective on "Density functional approach to the frontier-electron theory of chemical reactivity", Theoretical Chemistry Accounts: Theory, Computation, and Modeling (Theoretica Chimica Acta) 103 (3-4) (2000) 353–360. doi:10.1007/s002149900093.

[60] Q. Wang, F. Li, X. Shen, W. Shi, X. Li, Y. Guo, S. Xiong, Q. Zhu, Relation between reactivity and electronic structure for α/L-, β- and γ-dicalcium silicate: A first-principles study, Cement and Concrete Research 57 (2014) 28–32. doi:10.1016/j.cemconres.2013.12.004.

[61] P. Rejmak, J. S. Dolado, M. A. G. Aranda, A. Ayuela, First-Principles Calculations on Polymorphs of Dicalcium Silicate—Belite, a Main Component of Portland Cement, The Journal of Physical Chemistry C 123 (11) (2019) 6768–6777.

doi:10.1021/acs.jpcc.8b10045.

[62] K. H. Jost, B. Ziemer, R. Seydel, Redetermination of the structure of β-dicalcium silicate, Acta Crystallographica Section B Structural Crystallography and Crystal Chemistry 33 (6) (1977) 1696–1700. doi:10.1107/s0567740877006918.

[63] Q. Wang, X. Gu, H. Zhou, X. Chen, X. Shen, Cation substitution induced reactivity variation on the tricalcium silicate polymorphs determined from first-principles calculations, Construction and Building Materials 216 (2019) 239–248. doi:10.1016/j.conbuildmat.2019.05.005.

[64] C. Qi, D. Spagnoli, A. Fourie, Structural, electronic, and mechanical properties of calcium aluminate cements: Insight from first-principles theory, Construction and Building Materials 264 (2020) 120259. doi:10.1016/j.conbuildmat.2020.120259.

[65] H. Manzano, Atomistic Simulation studies of the Cement Paste Components, Ph.D. thesis, University of the Basque Country (2009).

[66] J. S. Dolado, K. van Breugel, Recent advances in modeling for cementitious materials, Cement and Concrete Research 41 (7) (2011) 711–726. doi:10.1016/j.cemconres.2011.03.014.

[67] H. Minard, S. Garrault, L. Regnaud, A. Nonat, Mechanisms and parameters controlling the tricalcium aluminate reactivity in the presence of gypsum, Cement and Concrete Research 37 (10) (2007) 1418–1426. doi:10.1016/j.cemconres.2007.06.001.

[68] C. Qi, A. Fourie, Q. Chen, P. Liu, Application of first-principles theory in ferrite phases of cemented paste backfill, Minerals Engineering 133 (2019) 47–51. doi:10.1016/j.mineng.2019.01.011.

[69] X. M. Aretxabaleta, I. Etxebarria, H. Manzano, Electronic and elastic properties of brownmillerite, Materials Research Express 7 (1) (2020) 015516. doi:10.1088/2053-1591/ab61a1.

[70] H. Manzano, E. Durgun, M. J. A. Qomi, F.-J. Ulm, R. J. M. Pellenq, J. C. Grossman, Impact of Chemical Impurities on the Crystalline Cement Clinker Phases Determined by Atomistic Simulations, Crystal Growth & Design 11 (7) (2011) 2964–2972. doi:10.1021/cg200212c.

[71] K. Saritas, C. Ataca, J. C. Grossman, Predicting Electronic Structure in Tricalcium Silicate Phases with Impurities Using First-Principles, The Journal of Physical Chemistry C 119 (9) (2015) 5074–5079. doi:10.1021/jp510597e.

[72] J. Huang, L. Valenzano, T. V. Singh, R. Pandey, G. Sant, Influence of (Al, Fe, Mg) Impurities on Triclinic Ca3SiO5: Interpretations from DFT Calculations, Crystal Growth & Design 14 (5) (2014) 2158–2171. doi:10.1021/cg401647f.

[73] L. Nicoleau, E. Schreiner, A. Nonat, Ion-specific effects influencing the dissolution of tricalcium silicate, Cement and Concrete Research 59 (2014) 118–138. doi:10.1016/j.cemconres.2014.02.006.

[74] I. Odler, J. Schüppstuhl, Early hydration of tricalcium silicate III. control of the induction period, Cement and Concrete Research 11 (5-6) (1981) 765–774. doi:10.1016/0008-8846(81)90035-1.

[75] D. Stephan, S. N. Dikoundou, G. Raudaschl-Sieber, Influence of combined doping of tricalcium silicate with MgO, Al2O3 and Fe2O3: synthesis, grindability, X-ray diffraction and 29Si NMR, Materials and Structures 41 (10) (2008) 1729–1740. doi:10.1617/s11527-008-9360-3.

[76] P. Guo, B. Wang, M. Bauchy, G. Sant, Misfit Stresses Caused by Atomic Size Mismatch: The Origin of Doping-Induced Destabilization of Dicalcium Silicate, Crystal Growth & Design 16 (6) (2016) 3124–3132. doi:10.1021/acs.cgd.5b01740.

[77] Y. Tao, W. Zhang, D. Shang, Z. Xia, N. Li, W.-Y. Ching, F. Wang, S. Hu, Comprehending the occupying preference of manganese substitution in crystalline cement clinker phases: A theoretical study, Cement and Concrete Research 109 (2018) 19–29. doi:10.1016/j.cemconres.2018.04.003.

[78] Y. Tao, W. Zhang, N. Li, W.-Y. Ching, F. Wang, S. Hu, Atomic-level insights into the influence of zinc incorporation on clinker hydration reactivity, Open Ceramics (2020) 100004doi:10.1016/j.oceram.2020.100004.

[79] J. Zhu, K. Yang, Y. Chen, G. Fan, L. Zhang, B. Guo, X. Guan, R. Zhao, Revealing the substitution preference of zinc in ordinary Portland cement clinker phases: A study from experiments and DFT calculations, Journal of Hazardous

Materials (2020) 124504doi:10.1016/j.jhazmat.2020.124504.

[80] H. Bolio-Arceo, F. P. Glasser, Zinc oxide in cement clinkering: part 1. Systems CaO—ZnO—Al2O3and CaO—ZnO—Fe2O3, Advances in Cement Research 10 (1) (1998) 25–32. doi:10.1680/adcr.1998.10.1.25.

[81] P. W. Tasker, The stability of ionic crystal surfaces, Journal of Physics C: Solid State Physics 12 (22) (1979) 4977–4984. doi:10.1088/0022-3719/12/22/036.

[82] H. Manzano, E. Durgun, I. López-Arbeloa, J. C. Grossman, Insight on Tricalcium Silicate Hydration and Dissolution Mechanism from Molecular Simulations, ACS Applied Materials & Interfaces 7 (27) (2015) 14726–14733. doi:10.1021/acsami.5b02505.

[83] R. K. Mishra, R. J. Flatt, H. Heinz, Force Field for Tricalcium Silicate and Insight into Nanoscale Properties: Cleavage, Initial Hydration, and Adsorption of Organic Molecules, The Journal of Physical Chemistry C 117 (20) (2013) 10417–10432. doi:10.1021/jp312815g.

[84] C. Noguera, Polar oxide surfaces, Journal of Physics: Condensed Matter 12 (31) (2000) R367–R410. doi:10.1088/0953-8984/12/31/201.

[85] X. Chen, S. Wei, Q. Wang, M. Tang, X. Shen, X. Zou, Y. Shen, B. Ma, Morphology prediction of portlandite: Atomistic simulations and experimental research, Applied Surface Science 502 (2020) 144296. doi:10.1016/j.apsusc.2019.144296.

[86] Q. Wang, H. Manzano, I. López-Arbeloa, X. Shen, Water Adsorption on the β-Dicalcium Silicate Surface from DFT Simulations, Minerals 8 (9) (2018) 386. doi:10.3390/min8090386.

[87] E. Durgun, H. Manzano, P. V. Kumar, J. C. Grossman, The Characterization, Stability, and Reactivity of Synthetic Calcium Silicate Surfaces from First Principles, The Journal of Physical Chemistry C 118 (28) (2014) 15214–15219. doi:10.1021/jp408325f.

[88] J. Huang, B. Wang, Y. Yu, L. Valenzano, M. Bauchy, G. Sant, Electronic Origin of Doping-Induced Enhancements of Reactivity: Case Study of Tricalcium Silicate, The Journal of Physical Chemistry C 119 (46) (2015) 25991–25999. doi:10.1021/acs.jpcc.5b08286.

[89] M.-N. de Noirfontaine, F. Dunstetter, M. Courtial, G. Gasecki, M. Signes-Frehel, Polymorphism of tricalcium silicate, the major compound of Portland cement clinker, Cement and Concrete Research 36 (1) (2006) 54–64. doi:10.1016/j.cemconres.2004.12.004.

[90] W. G. Mumme, Crystal structure of tricalcium silicate from a Portland cement clinker and its application to quantitative XRD analysis, Neues Jahrbuch fuer Mineralogie: Monatshefte 4 (1995) 145–160.

[91] J. Claverie, F. Bernard, J. M. M. Cordeiro, S. Kamali-Bernard, Water's behaviour on Ca-rich tricalcium silicate surfaces for various degrees of hydration: A molecular dynamics investigation, Journal of Physics and Chemistry of Solids 132 (2019) 48–55. doi:10.1016/j.jpcs.2019.03.020.

[92] J. Claverie, S. Kamali-Bernard, J. M. M. Cordeiro, F. Bernard, Assessment of mechanical, thermal properties and crystal shapes of monoclinic tricalcium silicate from atomistic simulations, Cement and Concrete Research 140 (2021) 106269. doi:10.1016/j.cemconres.2020.106269.

[93] M.-N. D. Noirfontaine, M. Courtial, F. Dunstetter, G. Gasecki, M. Signes-Frehel, Tricalcium silicate Ca3SiO5 superstructure analysis: a route towards the structure of the M1 polymorph, Zeitschrift fÃ¼r Kristallographie 227 (2) (2012) 102–112.

[94] N. I. Golovastikov, R. G. Matveeva, N. V. Belov, Crystal structure of the tricalcium silicate $(CaOSiO_2)_3$=C_3S, Kristallografiya 20 (1975) 721–729.

[95] K. Fukuda, S. Ito, Improvement in Reactivity and Grindability of Belite-Rich Cement by Remelting Reaction, Journal of the American Ceramic Society 82 (8) (2004) 2177–2180. doi:10.1111/j.1151-2916.1999.tb02059.x.

[96] R. Czaya, Refinement of the structure of γ-Ca2SiO4, Acta Crystallographica Section B Structural Crystallography and Crystal Chemistry 27 (4) (1971) 848–849. doi:10.1107/s0567740871003030.

[97] S. Udagawa, K. Urabe, M. Natsume, T. Yano, Refinement of the crystal structure of γ-Ca2SiO4, Cement and Concrete Research 10 (2) (1980) 139–144. doi:10.1016/0008-8846(80)90070-8.

[98] P. Mondal, J. W. Jeffery, The crystal structure of tricalcium aluminate, Ca3Al2O6, Acta Crystallographica Section B Structural Crystallography and Crystal Chemistry 31 (3) (1975) 689–697. doi:10.1107/s0567740875003639.

[99] R. K. Mishra, L. Fernández-Carrasco, R. J. Flatt, H. Heinz, A force field for tricalcium aluminate to characterize surface properties, initial hydration, and organically modified interfaces in atomic resolution, Dalton Transactions 43 (27) (2014) 10602–10616. doi:10.1039/c4dt00438h.

[100] P. E. Blöchl, Projector augmented-wave method, Physical Review B 50 (24) (1994) 17953–17979. doi:10.1103/physrevb.50.17953.

[101] J. P. Perdew, K. Burke, M. Ernzerhof, Generalized Gradient Approximation Made Simple, Physical Review Letters 77 (18) (1996) 3865–3868. doi:10.1103/physrevlett.77.3865.

[102] S. Grimme, Semiempirical GGA-type density functional constructed with a long-range dispersion correction, Journal of Computational Chemistry 27 (15) (2006) 1787–1799. doi:10.1002/jcc.20495.

[103] F. P. Glasser, The Burning of Portland Cement, in: Lea's Chemistry of Cement and Concrete, Elsevier, 1998, pp. 195–240. doi:10.1016/b978-075066256-7/50017-5.

[104] Y. Zhang, X. Lu, D. Song, S. Liu, The adsorption of a single water molecule on low-index C3S surfaces: A DFT approach, Applied Surface Science 471 (2019) 658–663. doi:10.1016/j.apsusc.2018.12.063.

[105] Y. Zhang, X. Lu, D. Song, S. Liu, The adsorption behavior of a single and multi-water molecules on tricalcium silicate (111) surface from DFT calculations, Journal of the American Ceramic Society (sep 2018). doi:10.1111/jace.16093.

[106] C. Qi, L. Liu, J. He, Q. Chen, L.-J. Yu, P. Liu, Understanding Cement Hydration of Cemented Paste Backfill: DFT Study of Water Adsorption on Tricalcium Silicate (111) Surface, Minerals 9 (4) (2019) 202. doi:10.3390/min9040202.

[107] C. Qi, Q. Chen, A. Fourie, Role of Mg Impurity in the Water Adsorption over Low-Index Surfaces of Calcium Silicates: A DFT-D Study, Minerals 10 (8) (2020) 665. doi:10.3390/min10080665.

[108] J. Claverie, F. Bernard, J. M. M. Cordeiro, S. Kamali-Bernard, Ab initio molecular dynamics description of proton transfer at water-tricalcium silicate interface, Cement and Concrete Research 136 (2020) 106162. doi:10.1016/j.cemconres.2020.106162.

[109] Y. Zhang, X. Lu, Z. He, D. Song, Molecular and dissociative adsorption of a single water molecule on a β-dicalcium silicate (100) surface explored by a DFT approach, Journal of the American Ceramic Society (dec 2017). doi:10.1111/jace.15381.

[110] A. G. Kalinichev, J. Wang, R. J. Kirkpatrick, Molecular dynamics modeling of the structure, dynamics and energetics of mineral–water interfaces: Application to cement materials, Cement and Concrete Research 37 (3) (2007) 337–347. doi:10.1016/j.cemconres.2006.07.004.

[111] E. Pustovgar, R. P. Sangodkar, A. S. Andreev, M. Palacios, B. F. Chmelka, R. J. Flatt, J.-B. d'Espinose de Lacaillerie, Understanding silicate hydration from quantitative analyses of hydrating tricalcium silicates, Nature Communications 7 (2016) 10952. doi:10.1038/ncomms10952.

[112] G. Tocci, A. Michaelides, Solvent-Induced Proton Hopping at a Water-Oxide Interface, The Journal of Physical Chemistry Letters 5 (3) (2014) 474–480. doi:10.1021/jz402646c.

[113] S. Woutersen, H. J. Bakker, Ultrafast Vibrational and Structural Dynamics of the Proton in Liquid Water, Physical Review Letters 96 (13) (apr 2006). doi:10.1103/physrevlett.96.138305.

[114] E. Pustovgar, R. K. Mishra, M. Palacios, J.-B. d'Espinose de Lacaillerie, T. Matschei, A. S. Andreev, H. Heinz, R. Verel, R. J. Flatt, Influence of aluminates on the hydration kinetics of tricalcium silicate, Cement and Concrete Research 100 (2017) 245–262. doi:10.1016/j.cemconres.2017.06.006.

[115] L. Wang, D. Hou, H. Shang, T. Zhao, Molecular dynamics study on the Tri-calcium silicate hydration in sodium sulfate

solution: Interface structure, dynamics and dissolution mechanism, Construction and Building Materials 170 (2018) 402–417. doi:10.1016/j.conbuildmat.2018.03.035.

[116] A. Alex, A. K. Nagesh, P. Ghosh, Surface dissimilarity affects critical distance of influence for confined water, RSC Adv. 7 (6) (2017) 3573–3584. doi:10.1039/c6ra25758e.

[117] K. L. Scrivener, P. Juilland, P. J. M. Monteiro, Advances in understanding hydration of Portland cement, Cement and Concrete Research 78 (2015) 38–56. doi:10.1016/j.cemconres.2015.05.025.

[118] E. Dubina, L. Black, R. Sieber, J. Plank, Interaction of water vapour with anhydrous cement minerals, Advances in Applied Ceramics 109 (5) (2010) 260–268. doi:10.1179/174367509x12554402491029.

[119] L. Black, A. Stumm, K. Garbev, P. Stemmermann, K. R. Hallam, G. C. Allen, X-ray photoelectron spectroscopy of the cement clinker phases tricalcium silicate and β-dicalcium silicate, Cement and Concrete Research 33 (10) (2003) 1561–1565. doi:10.1016/s0008-8846(03)00097-8.

[120] F. Bellmann, T. Sowoidnich, H.-M. Ludwig, D. Damidot, Analysis of the surface of tricalcium silicate during the induction period by X-ray photoelectron spectroscopy, Cement and Concrete Research 42 (9) (2012) 1189–1198. doi:10.1016/j.cemconres.2012.05.011.

[121] V. Rheinheimer, I. Casanova, Hydration of C3S thin films, Cement and Concrete Research 42 (4) (2012) 593–597. doi:10.1016/j.cemconres.2012.01.002.

[122] V. Rheinheimer, I. Casanova, An X-ray photoelectron spectroscopy study of the hydration of C2S thin films, Cement and Concrete Research 60 (2014) 83–90. doi:10.1016/j.cemconres.2014.03.005.

[123] V. Rheinheimer, I. Casanova, Thin Films as a Tool for Nanoscale Studies of Cement Systems and Building Materials, in: Thin Film Processes - Artifacts on Surface Phenomena and Technological Facets, InTech, 2017. doi:10.5772/66665.

[124] O. Björneholm, M. H. Hansen, A. Hodgson, L.-M. Liu, D. T. Limmer, A. Michaelides, P. Pedevilla, J. Rossmeisl, H. Shen, G. Tocci, E. Tyrode, M.-M. Walz, J. Werner, H. Bluhm, Water at Interfaces, Chemical Reviews 116 (13) (2016) 7698–7726. doi:10.1021/acs.chemrev.6b00045.

[125] J. T. Newberg, D. E. Starr, S. Yamamoto, S. Kaya, T. Kendelewicz, E. R. Mysak, S. Porsgaard, M. B. Salmeron, G. E. Brown, A. Nilsson, H. Bluhm, Autocatalytic Surface Hydroxylation of MgO(100) Terrace Sites Observed under Ambient Conditions, The Journal of Physical Chemistry C 115 (26) (2011) 12864–12872. doi:10.1021/jp200235v.

[126] M. Ončák, R. Włodarczyk, J. Sauer, Hydration Structures of MgO, CaO, and SrO (001) Surfaces, The Journal of Physical Chemistry C 120 (43) (2016) 24762–24769. doi:10.1021/acs.jpcc.6b07434.

[127] X. Deng, T. Herranz, C. Weis, H. Bluhm, M. Salmeron, Adsorption of Water on Cu2O and Al2O3 Thin Films, The Journal of Physical Chemistry C 112 (26) (2008) 9668–9672. doi:10.1021/jp800944r.

[128] Y. Fujimori, X. Zhao, X. Shao, S. V. Levchenko, N. Nilius, M. Sterrer, H.-J. Freund, Interaction of Water with the CaO(001) Surface, The Journal of Physical Chemistry C 120 (10) (2016) 5565–5576. doi:10.1021/acs.jpcc.6b00433.

[129] A. Verdaguer, C. Weis, G. Oncins, G. Ketteler, H. Bluhm, M. Salmeron, Growth and Structure of Water on SiO2 Films on Si Investigated by Kelvin Probe Microscopy and in Situ X-ray Spectroscopies, Langmuir 23 (19) (2007) 9699–9703. doi:10.1021/la700893w.

[130] S. Yamamoto, T. Kendelewicz, J. T. Newberg, G. Ketteler, D. E. Starr, E. R. Mysak, K. J. Andersson, H. Ogasawara, H. Bluhm, M. Salmeron, G. E. Brown, A. Nilsson, Water Adsorption on α-Fe2O3(0001) at near Ambient Conditions, The Journal of Physical Chemistry C 114 (5) (2010) 2256–2266. doi:10.1021/jp909876t.

[131] H. Söngen, C. Marutschke, P. Spijker, E. Holmgren, I. Hermes, R. Bechstein, S. Klassen, J. Tracey, A. S. Foster, A. Kühnle, Chemical Identification at the Solid–Liquid Interface, Langmuir 33 (1) (2016) 125–129. doi:10.1021/acs.langmuir.6b03814.

[132] B. Reischl, P. Raiteri, J. D. Gale, A. L. Rohl, Atomistic Simulation of Atomic Force Microscopy Imaging of Hydration Layers on Calcite, Dolomite, and Magnesite Surfaces, The Journal of Physical Chemistry C 123 (24) (2019) 14985–14992.

doi:10.1021/acs.jpcc.9b00939.

[133] H. Manzano, Dissolution mechanism and activation energies of alite and lime from molecular dynamics simulations, in: 15th International Congress on the Chemistry of Cement, 2019.

[134] P. Martin, H. Manzano, J. S. Dolado, Mechanisms and Dynamics of Mineral Dissolution: A New Kinetic Monte Carlo Model, Advanced Theory and Simulations 2 (10) (2019) 1900114. doi:10.1002/adts.201900114.

[135] P. Martin, J. J. Gaitero, J. S. Dolado, H. Manzano, KIMERA: A Kinetic Montecarlo Code for Mineral Dissolution, Minerals 10 (9) (2020) 825. doi:10.3390/min10090825.

[136] J. Chen, P. Martin, Z. Xu, H. Manzano, J. S. Dolado, G. Ye, A dissolution model of alite coupling surface topography and ions transport under different hydrodynamics conditions at microscale, Cement and Concrete Research 142 (2021) 106377. doi:10.1016/j.cemconres.2021.106377.

[137] K. Coopamootoo, E. Masoero, Simulations of Crystal Dissolution Using Interacting Particles: Prediction of Stress Evolution and Rates at Defects and Application to Tricalcium Silicate, The Journal of Physical Chemistry C 124 (36) (2020) 19603–19615. doi:10.1021/acs.jpcc.0c04633.

[138] I. Shvab, L. Brochard, H. Manzano, E. Masoero, Precipitation Mechanisms of Mesoporous Nanoparticle Aggregates: Off-Lattice, Coarse-Grained, Kinetic Simulations, Crystal Growth & Design 17 (3) (2017) 1316–1327. doi:10.1021/acs.cgd.6b01712.

[139] L. Nicoleau, A. Nonat, D. Perrey, The di- and tricalcium silicate dissolutions, Cement and Concrete Research 47 (2013) 14–30. doi:10.1016/j.cemconres.2013.01.017.

[140] D. J. Earl, M. W. Deem, Parallel tempering: Theory, applications, and new perspectives, Physical Chemistry Chemical Physics 7 (23) (2005) 3910. doi:10.1039/b509983h.

[141] R. Dupuis, D. G. Rodrigues, J.-B. Champenois, R. Pellenq, A. Poulesquen, Time resolved alkali silicate decondensation by sodium hydroxide solution, Journal of Physics: Materials (nov 2019). doi:10.1088/2515-7639/ab5ce9.

[142] R. Dupuis, L. K. Béland, R. J.-M. Pellenq, Molecular simulation of silica gels: Formation, dilution, and drying, Physical Review Materials 3 (7) (2019) 075603. doi:10.1103/physrevmaterials.3.075603.